HOKKAIDO UNIVERSITY

Title	Chelatase activity of magnesium dechelatase associated with chlorophyll degradation
Author(s)	Sato, Soma; Hirose, Mitsuaki; Tamiaki, Hitoshi et al.
Citation	FEBS Letters, 599(15), 2210-2219 https://doi.org/10.1002/1873-3468.70094
Issue Date	2025-06-17
Doc URL	https://hdl.handle.net/2115/97899
Rights	This is the peer reviewed version of the following article: Sato, S., Hirose, M., Tamiaki, H. and Ito, H. (2025), Chelatase activity of magnesium dechelatase associated with chlorophyll degradation. FEBS Lett, 599: 2210-2219., which has been published in final form at https://doi.org/10.1002/1873-3468.70094 This article may be used for non-commercial purposes in accordance with Wiley Terms and Conditions for Use of Self-Archived Versions. This article may not be enhanced, enriched or otherwise transformed into a derivative work, without express permission from Wiley or by statutory rights under applicable legislation. Copyright notices must not be removed, obscured or modified. The article must be linked to Wiley's version of record on Wiley Online Library and any embedding, framing or otherwise making available the article or pages thereof by third parties from platforms, services and websites other than Wiley Online Library must be prohibited.
Type	journal article
File Information	2025-FEBS.pdf

Hokkaido University Collection of Scholarly and Academic Papers : HUSCAP

Title

Chelatase activity of magnesium dechelatase associated with chlorophyll degradation

Authors

Soma Sato[1, 2], Mitsuaki Hirose[3, 4], Hitoshi Tamiaki[3], Hisashi Ito[2 *]

1 Graduate School of Environmental Science, Hokkaido University, N10 W5, Sapporo 060-0810, Japan

2 Institute of Low Temperature Science, Hokkaido University, N19 W8, Sapporo 060-0819, Japan

3 Graduate School of Life Sciences, Ritsumeikan University, Kusatsu, Shiga 525-8577, Japan

4 Department of Science and Technology, Seikei University, Tokyo, 180-8633, Japan

*Corresponding author

Hisashi Ito

Institute of Low Temperature Science, Hokkaido University, N19 W8, Sapporo 060-0819, Japan

Tel; +81-11-706-5469

E-mail; ito98@lowtem.hokudai.ac.jp

Keywords

chelatase, dechelatase, metal ion, substrate specificity

Abbreviations

AbSGR-h, *Anaerolineae* bacterium SM23_63 SGR homolog; AtSGRL, *Arabidopsis thaliana* SGR Like; βDDM, dodecyl β-maltoside; HPLC, high-performance liquid chromatography; Me-pyroPheide *a*, methyl pyropheophorbide *a*; SGR, stay green.

Running heading

Chelatase activity of magnesium dechelatase

Abstract
Metalated tetrapyrrole molecules play crucial roles in respiration, photosynthesis, and biocatalysis. In this study, the chelatase activity of the bacterial magnesium dechelatase homologous gene, which encodes an enzyme that extracts the central magnesium ion from chlorophyll, was demonstrated. The recombinant protein inserted metal ions, such as zinc, into methyl pyropheophorbide *a*, a synthetic derivative of chlorophyll *a*. Mutation analysis and structural modeling suggested H32, D34, and D62 as key residues involved in coordinating metal ions and facilitating proton extraction from methyl pyropheophorbide *a*. Chelatase activity was also found in the recombinant plant magnesium dechelatase protein. The bacterial gene complemented *Escherichia coli* ferrochelatase mutants. These findings provide novel insights into the mechanisms underlying chelation reactions.

Introduction

Cyclic tetrapyrrole molecules containing metal ions at their center are essential for living organisms and are used as cofactors and prosthetic groups in the metabolic pathway. Iron (Fe), cobalt (Co), nickel (Ni), zinc (Zn), and magnesium (Mg) ions are used to form functional tetrapyrroles [1-3]. When a Fe ion is inserted into protoporphyrin IX, coproporphyrin III, or sirohydrochlorin, heme is produced as the end product. Vitamin B_{12} and coenzyme F_{430} are produced when Co and Ni ions are inserted into sirohydrochlorin, respectively. Inserting Mg ions into protoporphyrin IX leads to the formation of various chlorophyll molecules essential for photosynthesis. Zn bacteriochlorophyll is a photosynthetic pigment in photosynthetic bacteria living under acidic conditions [4]. The chelatases that catalyze these reactions are ATP-dependent or -independent [1]. The ATP demand depends on the ease with which the chemical reaction proceeds. Mg chelatase is an ATP-dependent enzyme [5], whereas ferrochelatase is ATP-independent [6]. Mg insertion is an energetically unfavorable reaction since hydrated Mg ions are stable, whereas Fe ion insertion is energetically favorable as Fe-tetrapyrrole complexes are stable.

While metal ion insertion is a well-characterized enzymatic process, the mechanisms of metal extraction vary, with some steps occurring spontaneously and others being facilitated by different enzymes. The first step in heme degradation is the oxidative cleavage of the tetrapyrrole macrocyclic ring by heme oxygenase [7], after which the Fe ion is spontaneously released. Although chlorophyll has a similar structure to heme, the extraction of Mg from chlorophyll differs from heme degradation. Mg is first removed from chlorophyll by Mg dechelatase, and the tetrapyrrole ring is

oxidatively cleaved [8].

Mg dechelatase has been identified in stay-green rice mutants, which have defects in chlorophyll degradation and retain green leaves during senescence [9]. Therefore, the gene encoding Mg dechelatase is stay-green (*SGR* or Non Yellowing1; *NYE1*). Although SGR is involved in chlorophyll degradation in green plants, homologous *SGR* genes have been identified in some non-photosynthetic bacterial genomes [10]. The recombinant protein of the *SGR* homologous gene derived from the *Anaerolineae* bacterium SM23_63 (AbSGR-h) has been characterized for its enzymatic properties, and its crystal structure has been determined [11,12]. Analysis of the amino acid substitution mutations suggested the involvement of aspartate and histidine residues in Mg extraction. However, the physiological functions of the *SGR* homolog in bacterial cells remain to be fully elucidated, and the reaction mechanism of Mg dechelatase remains nebulous.

In this study, we investigated the chelatase activity of dechelatase to understand the metal ion insertion/extraction mechanisms and found that AbSGR-h inserted copper (Cu) and Zn into an unnatural and synthetic chlorophyll *a* derivative, methyl pyropheophorbide *a* (Me-pyroPheide *a*) (Fig. S1). Manganese (Mn), Fe, Co, and Ni were also inserted, albeit with lower efficiencies. This study provides novel insights into the mechanism underlying the enzymatic metalation/demetalation reaction.

Materials and Methods

Cloning of bacterial *SGR* homologs and recombinant protein preparation

The bacterial *SGR* homolog from AbSGR-h, encoded by *KPK94580* with codon usage optimized for *E. coli* was artificially synthesized and cloned into pET 30a (+) vectors (Novagen) containing a histidine tag at the C-terminus [12]. The H102A mutation was introduced by polymerase chain reaction (PCR) using the primers listed in Table S1, as previously described [12]. The constructed plasmids were introduced into *E. coli* BL21 (DE3) cells for protein expression. *E. coli* was grown, and the recombinant protein was expressed in an autoinduction medium [13]. After induction of the recombinant protein, the cultured cells were harvested using centrifugation at 7,000 × *g* for 5 min. Harvested cells were resuspended in buffer A (25 mM Tris-HCl pH 7.5, 100 mM NaCl, and 20 mM imidazole) and disrupted by sonication (Branson Sonifier SFX250: output 8, duty cycle 20%) for 6 min in an ice bath. Following sonication, dodecyl β-maltoside (βDDM) was added to a final concentration of 0.05% (w/v) and incubated at 25 °C for 10 min. The clarified cell lysate supernatant was obtained via centrifugation at 20,000 × *g* for 10 min two times and applied to a 5 mL HisTrap HP column (Cytiva) equilibrated with buffer A

containing 0.05% βDDM. The recombinant proteins were eluted using buffer B (25 mM Tri-HCl pH 7.5, 100 mM NaCl, 500 mM imidazole, and 0.05% βDDM) using an ÄKTAprime plus system (Cytiva). The purified protein (1 µg) was subjected to sodium dodecyl sulfate polyacrylamide gel electrophoresis to verify protein purity. *Arabidopsis thaliana* SGR Like (AtSGRL) with a FATT tag was expressed and purified as previously described [10].

Enzymatic assay

Purified protein was diluted in buffer (25 mM Tri-HCl pH 7.5, 100 mM NaCl, and 0.05% βDDM) for each experiment. Me-pyroPheide *a* was prepared by substituting the phytyl group with a methyl group and removing the C13^2-methoxycarbonyl group from pheophytin *a* (11). Protein (10 µM), Me-pyroPheide *a* (40 µM), and 100 µM of metal ions were incubated for 15 h at 25 °C to investigate the insertion of different metal ions. Ferrous ions were prepared by adding small granules of dithionite to a $FeCl_3$ solution. Pigments were analyzed through high-performance liquid chromatography (HPLC) equipped with a diode array detector to monitor on-line visible absorption spectroscopy (SPD-M20A, Shimadzu) on a C8 column (4.6 ϕ × 150 mm, Waters Symmetry C8, Waters) with eluent A (0.25 M aqueous pyridine solution: methanol: acetonitrile [1:2:1 v:v:v]) and eluent B (methanol: acetonitrile: acetone [1:3:1 v:v:v]) (1:1) [14] at a flow rate of 1 mL min^{-1} at 40 °C. Protein (10 µM) and chlorophyll *a* (5 µM) were incubated for 30 min at 25 °C to investigate Mg extraction from chlorophyll *a* using the mutant enzyme. The pigments were then analyzed via HPLC using only eluent B. To investigate Zn insertion using the mutant enzyme, 10 µM protein, 2.5 µM $ZnCl_2$, and 5 µM Me-pyroPheide *a* were incubated for 30 min at 25 °C. To obtain enzymatic parameters, 0.05 µM protein was used and incubated for 5 min. The kinetic (k_{cat}) and affinity (K_m) values were obtained by fitting the data to a Michaelis–Menten plot using Solver (Excel, Microsoft). As the C13^2-methoxycarbonyl and O17^4-phytyl groups in chlorophyll derivatives have marginal effects on spectroscopic properties, Zn and Cu complexes were quantified using the molar extinction coefficients of Zn (ε = 90.3 mM^{-1} cm^{-1} at 658 nm) and Cu pheophytins *a* (ε = 67.9 mM^{-1} cm^{-1} at 650 nm) [15]. The molar extinction coefficients of Me-pyroPheide *a* is the same as that of pheophytin *a* (ε = 52.6 mM^{-1} cm^{-1} at 664 nm). Atmospheric pressure chemical ionization-Orbitrap mass spectrometry (Thermo Scientific Exactive Plus, Thermo Fisher Scientific) was used to determine the mass of the metal complexes.

Metal ion insertion by non-enzymatic reactions

Me-pyroPheide *a* was dissolved in a small volume of dimethyl sulfoxide and diluted with methanol. Me-pyroPheide *a* (5 μM), and $ZnCl_2$ or $CuCl_2$ (500 μM) were prepared in methanol, and the absorbance at 413 nm was recorded every 5 min (Multiskan GO, Thermo Scientific). The half-life was calculated using Solver (Excel).

Complementation of *hemH E. coli*

hemH-defective *E. coli* mutants (VS200), in which bases 468 to 874 of ferrochelatase are deleted [16], were obtained from the National BioResource Project of Japan. *E. coli* JM109 *hemH* and *AbSGR-h* were amplified using specific primer sets (Table S1) and inserted into pUC119 at the *Hind*III and *Eco*RI sites. *E. coli* was transformed with the plasmids and cultured on Luria–Bertani agar medium containing 25 μg mL^{-1} ampicillin with or without 0.2% glucose (w/v) for 2 days at 37 °C in the dark. *E. coli* carrying an empty vector served as a negative control.

Results

Examination of the metal insertion activity of AbSGR-h

The metal insertion activity of AbSGR-h was investigated using Me-pyroPheide *a* as the macrocycle tetrapyrrole molecule since it lacks stereoisomerism at the peripheral $C13^2$-position [17], allowing for the accurate identification of the reaction products. This molecule was prepared by substituting the phytyl group to a methyl group in the C17-propionate residue and removing the $C13^2$-methoxycarbonyl group from pheophytin *a* [18]. Me-pyroPheide *a* and Mn, Fe, Co, Ni, Cu, and Zn were incubated with AbSGR-h in an aqueous solution at 25 °C, and the pigments were analyzed (Fig. 1, Fig. S2). The purity of AbSGR-h was determined using gel electrophoresis (Fig. S3). Following incubation, new pigments were observed in HPLC, the identities of which were determined using mass spectrometry (Fig. S4). All the produced pigments had masses corresponding to each metalated molecule. The Mn and Co complexes formed low and broad peaks in the HPLC chromatogram (Fig. 1). Mn complexes can take various oxidation states [19], affecting the pigment retention time. The absorption spectrum (Fig. S2) and mass spectra (Fig. S4) of the Mn complex suggested that the analyzed Mn was Mn^{3+}. Mass spectrometry also suggested Fe to be Fe^{3+} (Fig. S4). Though Co can also be Co^{3+} [20], mass spectrometry suggested that Co^{2+} was dominant. It is unclear why the Co complex has a broader peak in the HPLC chromatogram. When the Qy wavelengths of these molecules are ordered from shortest to longest, the order is consistent with that of metal chlorins in previous studies, Fe < Ni ≤ Co < Cu < Zn < Mn [21,22]. These observations support the accuracy of metal complex identification.

To exclude the possibility of non-enzymatic formation of the metal complexes, metal ions and Me-pyroPheide *a* were incubated without AbSGR-h; no metal complexes were formed (Fig. S5), suggesting that the formation of metal complexes is an enzymatic reaction. These results indicate that AbSGR-h can insert Mn, Fe, Co, Ni, Cu, and Zn into Me-pyroPheide *a* with particularly high efficiency for Cu and Zn.

Characterization of enzymatic properties against Cu and Zn

Cu and Zn were efficiently inserted; therefore, the enzymatic properties of these two metal ions were investigated (Fig. S6). AbSGR-h concentrations were set at 0.05 μM and incubated for 5 min. Under these reaction conditions, the reaction product increases proportionately to the reaction time (Fig. S6A and B). To examine the affinity and kinetics of metal ion insertion, 5 μM of Me-pyroPheide *a* was used. The K_m values for Cu and Zn were 2.29 ± 0.28 μM and 1.01 ± 0.32 μM, and the k_{cat} values for Cu and Zn were 2.03 ± 0.12 min^{-1} and 2.22 ± 0.43 min^{-1}, respectively (Table 1). High Zn concentrations suppressed the metalated molecule production; therefore, the Zn concentration was maintained below 2.5 μM. Metal ions (2.5 μM) were used to examine the affinity and kinetics of Me-pyroPheide *a*. The K_m values for Cu and Zn were 4.43 ± 0.07 μM and 2.46 ± 0.19 μM and the k_{cat} values for Cu and Zn were 2.55 ± 0.38 min^{-1} and 2.81 ± 0.25 min^{-1}, respectively (Table 2). These results suggest that Zn is the preferred metal ion for the AbSGR-h reaction. Non-enzymatic metalation was also examined in methanol; Cu was preferred for the reaction (Fig. S7), suggesting that the high affinity of Zn to AbSGR-h plays an important role in the enzymatic chelation activity.

Effects of AbSGR-h amino acid substitution on dechelation and chelation activity

Mutants were constructed by substituting the conserved amino acid residues in the active site. The mutants targeted three amino acid residues (H32, D34, and D62) previously suggested to be involved in the AbSGR-h metal extraction reaction [12]. H102, which is located in the active site, was also mutated. This histidine residue is often substituted by a glutamate residue in the SGR family proteins. In the Mg-dechelation reaction of chlorophyll *a* to pheophytin *a*, the D34N and D62N mutants showed almost no activity, whereas the H32A mutant showed lower activity, consistent with previous findings [12] (Fig. 2A, Fig. S8A). The H102A mutant exhibited no apparent decrease in Mg extraction activity.

In the Zn chelation reaction of Me-pyroPheide *a*, the H32A, D34N, and D62N mutants lost their enzymatic activity (Fig. 2B, Fig. S8B). However, the H102A mutant retained

chelation activity. Thus, H32, D34, and D62 were involved in the chelation reaction of AbSGR-h, with H32 playing a more prominent role in the chelation reaction than in the dechelation reaction under the experimental conditions. H102 appeared to have little effect on the activity in both reactions.

Examination of the metal insertion activity of plant *SGR*

AtSGRL recombinant protein was incubated with Zn ions and Me-pyroPheide *a* to examine the metal insertion activity of plant SGR. Arabidopsis has three SGR family proteins: AtSGR1, AtSGR2, and AtSGRL. Since AtSGR1 and AtSGR2 recombinant proteins are not expressed in *E. coli*, AtSGRL was used for this assay. As the AtSGRL expression level in *E. coli* and its purity after Ni affinity column purification were low (Fig. S3), the enzymatic activity could not be normalized by protein concentration. In addition to Mg extraction from chlorophyll *a* (Fig. 3A), Zn insertion into Me-pyroPheide *a* (Fig. 3B) was observed, indicating that plant *SGR* can also insert metal ions into macrocyclic tetrapyrrole molecules.

Complementation of *hemH*-defective *E. coli*

A bacterial *SGR* homolog was used to investigate the catalytic mechanisms of *SGR*. However, the physiological functions of the bacterial *SGR* homolog in bacterial cells remain to be elucidated. The metal insertion activity observed in this study suggests that the bacterial *SGR* homolog functions as a ferrochelatase in cells. To test this hypothesis, AbSGR-h was expressed in an *E. coli* strain defective in *hemH*, which encodes a ferrochelatase. Mutant *E. coli* cannot produce heme and thus cannot grow without glucose supplementation. Following incubation for 2 days, the transformants grew on the agar medium without glucose supplementation (Fig. 4). These observations demonstrate that the bacterial *SGR* homolog functions as a ferrochelatase in bacterial cells.

Discussion

Identification of *SGR* chelatase activity

SGR was first identified as the gene responsible for the stay-green rice mutation; however, its function was unknown [9]. The Mg-extracting activity from chlorophyll was later demonstrated through an *in vitro* assay using a recombinant protein of Arabidopsis *SGR* prepared using a cell-free protein synthesis system [23]. Consequently, SGR has been studied as a catabolic enzyme involved in the chlorophyll degradation pathway [8]. This study demonstrated that SGR could also catalyze the

reverse reaction by inserting a metal ion into a macrocyclic tetrapyrrole molecule. The enzymatic activity of SGR has been investigated using recombinant proteins derived from bacterial genes [11] as plant SGRs have not been successfully expressed in *E. coli*. Although this study used a bacterial *SGR* homolog, metal insertion was also observed in plant *SGR* (Fig. 3). Therefore, SGR proteins are believed to insert and extract metal ions via the same reaction mechanism, regardless of whether the gene is derived from plants or bacteria. Notably, *in vitro* metalation activity does not necessarily reflect *in vivo* activity. Indeed, intracellularly, the metal availability often follows the inverse of the Irving–Williams series, with more competitive metals maintained at low availability [24,25]. In this study, AbSGR-h and AtSGRL efficiently inserted Zn *in vitro*; however, Zn concentrations are tightly regulated and maintained at low levels in plant cells by Zn transporters [26], suggesting that Zn insertion in chloroplasts is minimal. Moreover, in cellular environments, metal ions can be associated with ligands rather than existing in hydrated forms as in *in vitro* assays. These ligand-bound forms are more favorable for metalation since they bypass the energy cost of dehydration [25], limiting the applicability of *in vitro* results to *in vivo* conditions.

In this study, all metal ions were assumed to be in their divalent states at the start of the reactions; Fe^{2+} was prepared by adding dithionite to an $FeCl_3$ solution. Although Fe^{2+} is readily oxidized to Fe^{3+} (mass spectrometry; Fig. S4), Fe^{2+} is presumed to be the biologically relevant substrate for the enzymatic reaction, consistent with its *in viv*o roles. Similarly, while copper is most stable in the hydrated state at divalent and thus Cu^{2+} was used in the *in vitro* assays, copper exists predominantly as Cu^{+} in cells [27], implying that the kinetic parameters for copper in Tables 1 and 2 may differ under physiological conditions. *In vitro* assays using recombinant proteins can aid in elucidating enzymatic mechanisms and enzyme engineering. However, it is essential to recognize the limitations of such systems in fully capturing the enzyme's function within the cellular context.

Metal ion specificity for AbSGR-h enzymatic reactions

To determine the metal ion preference of AbSGR-h, we investigated the insertion efficiency of various metal ions into Me-pyroPheide *a*, resulting in the finding that Zn is the most favorable metal ion. Cu was preferred when Zn or Cu was coordinated to Me-pyroPheide *a* in methanol (Fig. S7), consistent with the Irving–Williams series and a previous study using porphyrins [28].

However, AbSGR-h preferred Zn over Cu for insertion into Me-pyroPheide *a* (Tables 1 and 2). The higher insertion rate of Zn may be attributed to the higher affinity of

AbSGR-h for Zn than Cu ions. Computational prediction of the complex structure using AlphaFold3 [29] suggested that SGR coordinates Zn ions with H32, D34, D62, and H102 to form a tetrahedral geometry (Fig. S9A). Zinc complexes typically have a tetrahedral geometry, whereas cupric complexes tend to have a square-planar geometry. The arrangement of these four amino acid residues may be favorable for Zn. However, Cu is the most favorable ion when amino acid residues coordinate with first-row transition metal ions, regardless of the overall symmetry of the binding site [30,31]. Although these observations suggest that Cu is the better metal ion, some chelatases, such as yeast ferrochelatase, also prefer Zn over Cu [32]. The reason AbSGR-h prefers Zn ions to Cu insertion remains unclear. Mn, Fe, Co, and Ni were inserted into Me-pyroPheide *a* using AbSGR-h; however, the efficiency was low (Fig. 1), potentially due to the lower insertion rate of metal ions into Me-pyroPheide *a,* as reported previously using porphyrin in an organic solution [28] rather than the affinity to AbSGR-h. Notably, AbSGR-h successfully formed a Mn complex (Fig. 1). Mn is the least favorable metal ion in the Irving-Williams series, and Mn-chelated complexes are not used in living organisms. AbSGR-h inserted Mn into Me-pyroPheide *a*, suggesting that AbSGR-h is a highly efficient enzyme. The molecular mechanisms underlying the broad substrate specificity of AbSGR-h remain to be elucidated.

Predicted structures and reaction mechanism of AbSGR-h

The amino acid residues involved in chelatase coordination of metal ions vary based on the chelatase species. Human ferrochelatase interacts with Fe using methionine, arginine, and tyrosine [33], whereas methionine is substituted with tyrosine in Bacillus ferrochelatase [34]. Bacterial Co and Ni chelatases use two histidine residues and one glutamate residue [35,36]. Although these essential amino acid residues are not found in SGR and the overall structure of SGR differs from that of chelatase [37], the coordination of the metal ion with the amino acid residues is consistent with that of Co or Ni chelatases. Histidine residues, such as H263 in human ferrochelatase, may be involved in proton extraction reactions [6]. H102 in AbSGR-h corresponds to H263 in human ferrochelatase. H102, or a substituted glutamic acid in some SGRs, can accept protons from the free base; however, mutation of this histidine residue did not significantly decrease enzymatic activity in either the insertion or extraction of metal ions (Fig. 2). These observations suggest that H102 is not involved in the transfer of protons between the enzyme and the substrate. Therefore, H32, D34, and D62 should accept protons from Me-pyroPheide *a* in the chelation reaction of AbSGR-h, indicating that the proton should be extracted from the same plane as the metal insertion (Fig.

S9B). Similar results have been reported for Mg chelatase [5]. H1174 of *Synechocystis* PCC6803 Mg chelatase is localized at the opposite site of Mg insertion and is not essential for the enzymatic reaction. These metal insertion–proton extraction mechanisms suggest that conventional free base distortion is not expected during this reaction. Such a free base distortion promotes the abstraction of two protons from the free base and exposes the pyrrole nitrogen atoms to the incoming metal ion substrate [1]. In this model, protons are received by the amino acid residue that localizes to the opposite site of the metal ion insertion. AbSGR-h does not have the corresponding amino acid residue; therefore, Me-pyroPheide *a* distortion does not promote the reaction. Elucidating the proton-transfer mechanism is crucial for understanding the chelation mechanism. AbSGR-h is a smaller and simpler enzyme than Mg chelatase, a heterotrimeric and ATP-dependent enzyme [5]. Therefore, AbSGR-h is a good enzyme for investigating metal- and proton-exchange processes.

The H32A mutation resulted in the loss of chelatase activity but retained a certain level of dechelatase activity (Fig. 2), suggesting that H32 plays different roles in chelation and dechelation reactions. However, the difference in the effect of H32 substitution could have been caused by the use of different substrates, namely chlorophyll *a* and Me-pyroPheide *a*. In human chelatases, substituting essential histidine and glutamate residues alters the enzymatic activity, which depends on the substrate [38]. This finding suggests that caution should be exercised when generalizing the role of amino acid residues in enzymatic reactions based on observations using different substrates. Further analyses of these mutations will provide deeper insights into the underlying reaction mechanisms.

The acidic side group of the free base plays an essential role in chelatase substrate specificity [6]. For example, protoporphyrin IX, a substrate for both ferrochelatases and Mg chelatases, contains two polar propionate groups, which interact with basic amino acid residues or main chain amides [5,39]. This study used an artificial substrate without acidic side groups. Side-chain modification of the Mg complex does not significantly affect the dechelation reaction catalyzed by AbSGR-h as long as the side-chain size is not markedly different [18]. These observations suggest that SGR accepts different substrates, regardless of the polarity of the side groups. The broad substrate specificity of SGR is excellent for developing new enzymes.

Ferrochelatase activity of AbSGR-h

SGR-homologous genes have been identified in some non-photosynthetic bacteria [10]; however, their physiological functions in bacterial cells have not yet been

elucidated. In the present study, AbSGR-h successfully complemented a ferrochelatase mutant *E. coli* (Fig. 4), suggesting that *SGR*-homologous genes have the potential to participate in heme biosynthesis as ferrochelatases. The ferrous ion insertion into Me-pyroPheide *a* activity *in vitro* was not significant (Fig. 1). Ferrous ions are easily oxidized in solution [32], which may affect chelatase activity *in vitro*. Protoporphyrin IX, the substrate for heme biosynthesis in *E. coli*, has not been examined using *in vitro* assays. Metal ion insertion rates can differ from those into Me-pyroPhdeide *a*. Although AbSGR-h showed high activity with Zn, this finding does not imply that Zn is a physiological metal ion. Human ferrochelatase prefers Zn to Fe *in vitro* [40]. This study demonstrated the *in vitro* activity of AbSGR-h. However, the function of the SGR homolog in bacterial cells, which was not investigated, and its function was established only by complementing the *E. coli* mutant lacking ferrochelatase. Whether bacterial SGR homologs exhibit chelatase activity in cells should be further investigated. Determining the physiological function of the SGR homolog will provide insights into the diversity of metal complex biosynthesis in living organisms.

Author Contributions

H. I. designed research; S. S. and H. I. performed research; M. H. and H. T. analyzed data; H. I. wrote the paper.

Data Accessibility

The data are contained within the article and Supporting Information section.

Acknowledgments

We thank Prof. Ryouichi Tanaka for valuable suggestions. Mass spectrometry was performed by Global Facility Center, Hokkaido University. This study was supported by the Japan Society for the Promotion of Science (JSPS) KAKENHI Grant Numbers JP21J22995 (to M.H.), JP22H02203 (to H.T.), JP23K23470 (to H.T.), and JP23K05691 (to H.I.).

Conflict of Interest

The authors declare no conflicts of interest.

[1] Al-Karadaghi S, Franco R, Hansson M, Shelnutt JA, Isaya G and Ferreira GC. (2006). Chelatases: distort to select? *Trends Biochem Sci* **31**, 135-142,

doi:10.1016/j.tibs.2006.01.001.

[2] Bryant DA, Hunter CN and Warren MJ. (2020). Biosynthesis of the modified tetrapyrroles-the pigments of life. *J Biol Chem* **295**, 6888-6925, doi:10.1074/jbc.REV120.006194.

[3] Layer G. (2021). Heme biosynthesis in prokaryotes. *Biochim Biophys Acta Mol Cell Res* **1868**, 118861, doi:10.1016/j.bbamcr.2020.118861.

[4] Wakao N, Yokoi N, Isoyama N, Hiraishi A, Shimada K, Kobayashi M, Kise H, Iwaki M, Itoh S and Takaichi S. (1996). Discovery of Natural Photosynthesis using Zn-Containing Bacteriochlorophyll in an Aerobic Bacterium Acidiphilium rubrum. *Plant Cell Physiol* **37**, 889-893, doi:10.1093/oxfordjournals.pcp.a029029.

[5] Adams NBP, Bisson C, Brindley AA, Farmer DA, Davison PA, Reid JD and Hunter CN. (2020). The active site of magnesium chelatase. *Nature Plants* **6**, 1491-1502, doi:10.1038/s41477-020-00806-9.

[6] Hunter GA and Ferreira GC. (2022). Metal ion coordination sites in ferrochelatase. *Coord Chem Rev* **460**, 214464, doi:10.1016/j.ccr.2022.214464.

[7] Beale SI. (1993). Biosynthesis of phycobilins. *Chem Rev* **93**, 785-802, doi:10.1021/cr00018a008.

[8] Tanaka A and Ito H. (2025). Chlorophyll Degradation and Its Physiological Function. *Plant Cell Physiol* **66**, 139-152, doi:10.1093/pcp/pcae093.

[9] Park SY, Yu JW, Park JS, Li J, Yoo SC, Lee NY, Lee SK, Jeong SW, Seo HS, Koh HJ *et al.* (2007). The senescence-induced staygreen protein regulates chlorophyll degradation. *Plant Cell* **19**, 1649-1664, doi:10.1105/tpc.106.044891.

[10] Obata D, Takabayashi A, Tanaka R, Tanaka A and Ito H. (2019). Horizontal Transfer of Promiscuous Activity from Nonphotosynthetic Bacteria Contributed to Evolution of Chlorophyll Degradation Pathway. *Mol Biol Evol* **36**, 2830-2841, doi:10.1093/molbev/msz193.

[11] Dey D, Nishijima M, Tanaka R, Kurisu G, Tanaka H and Ito H. (2022). Crystal structure and reaction mechanism of a bacterial Mg-dechelatase homolog from the Chloroflexi Anaerolineae. *Protein Sci* **31**, e4430, doi:10.1002/pro.4430.

[12] Dey D, Dhar D, Fortunato H, Obata D, Tanaka A, Tanaka R, Basu S and Ito H. (2021). Insights into the structure and function of the rate-limiting enzyme of chlorophyll degradation through analysis of a bacterial Mg-dechelatase homolog. *Comput Struct Biotechnol J* **19**, 5333-5347, doi:10.1016/j.csbj.2021.09.023.

[13] Studier FW. (2005). Protein production by auto-induction in high density shaking cultures. *Protein Expr Purif* **41**, 207-234, doi:10.1016/j.pep.2005.01.016

[14] Zapata M, Rodríguez F and Garrido JL. (2000). Separation of chlorophylls and

carotenoids from marine phytoplankton: a new HPLC method using a reversed phase C8 column and pyridine-containing mobile phases. *Mar Ecol Prog Ser* **195**, 29-45, doi:10.3354/meps195029.

[15] Jones ID, White RC, Gibbs E and Denard CD. (1968). Absorption spectra of copper and zinc complexes of pheophytins and pheophorbides. *J Agric Food Chem* **16**, 80-83, doi:10.1021/jf60155a001.

[16] Nakayashiki T and Inokuchi H. (1997). Effects of starvation for heme on the synthesis of porphyrins in *Escherichia coli*. *Molec Gen Genet* **255**, 376-381, doi:10.1007/s004380050509.

[17] Tamiaki H and Kichishima S. (2025). Chlorophyll Pigments and Their Synthetic Analogs. *Plant Cell Physiol* **66**, 153-167, doi:10.1093/pcp/pcae094.

[18] Sato S, Hirose M, Tanaka R, Ito H and Tamiaki H. (2024). In vitro demetalation of central magnesium in various chlorophyll derivatives using Mg-dechelatase homolog from the chloroflexi *Anaerolineae*. *Photosynth Res* **160**, 45-53, doi:10.1007/s11120-024-01088-4.

[19] Lomova T, Tsaplev Y, Klyueva M and Ovchenkova E. (2021). Recent advances in the practical use of the redox properties of manganese porphyrins. *J Organomet Chem* **945**, 121880, doi:10.1016/j.jorganchem.2021.121880.

[20] Li J, Noll BC, Oliver AG, Ferraudi G, Lappin AG and Scheidt WR. (2010). Oxygenation of Cobalt Porphyrinates: Coordination or Oxidation? *Inorg Chem* **49**, 2398-2406, doi:10.1021/ic902309f.

[21] Hirose M, Teramura M, Harada J and Tamiaki H. (2020). BciC-Catalyzed $C13^2$-Demethoxycarbonylation of Metal Pheophorbide *a* Alkyl Esters. *ChemBioChem* **21**, 1473-1480, doi:10.1002/cbic.201900745.

[22] Tamiaki H, Amakawa M, Holzwarth AR and Schaffner K. (2002). Aggregation of synthetic metallochlorins in hexane. A model of chlorosomal bacteriochlorophyll self-assemblies in green bacteria. *Photosynth Res* **71**, 59-67, doi:10.1023/A:1014951513848.

[23] Shimoda Y, Ito H and Tanaka A. (2016). Arabidopsis STAY-GREEN, Mendel's green cotyledon gene, encodes magnesium-dechelatase. *Plant Cell* **28**, 2147-2160, doi:10.1105/tpc.16.00428.

[24] Clough SE, Young TR, Tarrant E, Scott AJP, Chivers PT, Glasfeld A and Robinson NJ. (2025). A metal-trap tests and refines blueprints to engineer cellular protein metalation with different elements. *Nat Commun* **16**, 810, doi:10.1038/s41467-025-56199-w.

[25] Osman D and Robinson NJ. (2023). Protein metalation in a nutshell. *FEBS Lett*

597, 141-150, doi:10.1002/1873-3468.14500.

[26] Kolaj-Robin O, Russell D, Hayes KA, Pembroke JT and Soulimane T. (2015). Cation Diffusion Facilitator family: Structure and function. *FEBS Lett* **589**, 1283-1295, doi:10.1016/j.febslet.2015.04.007.

[27] Kardos J, Héja L, Simon Á, Jablonkai I, Kovács R and Jemnitz K. (2018). Copper signalling: causes and consequences. *Cell Commun Signal* **16**, 71, doi:10.1186/s12964-018-0277-3.

[28] Hambright P and Chock PB. (1974). Metal-porphyrin interactions. III. Dissociative-interchange mechanism for metal ion incorporation into porphyrin molecules. *J Am Chem Soc* **96**, 3123-3131, doi:10.1021/ja00817a018.

[29] Abramson J, Adler J, Dunger J, Evans R, Green T, Pritzel A, Ronneberger O, Willmore L, Ballard AJ, Bambrick J *et al.* (2024). Accurate structure prediction of biomolecular interactions with AlphaFold 3. *Nature* **630**, 493-500, doi:10.1038/s41586-024-07487-w.

[30] Dudev T and Lim C. (2014). Competition among Metal Ions for Protein Binding Sites: Determinants of Metal Ion Selectivity in Proteins. *Chem Rev* **114**, 538-556, doi:10.1021/cr4004665.

[31] McCall KA and Fierke CA. (2004). Probing Determinants of the Metal Ion Selectivity in Carbonic Anhydrase Using Mutagenesis. *Biochemistry* **43**, 3979-3986, doi:10.1021/bi0498914.

[32] Hunter GA, Sampson MP and Ferreira GC. (2008). Metal Ion Substrate Inhibition of Ferrochelatase. *J Biol Chem* **283**, 23685-23691, doi:10.1074/jbc.M803372200.

[33] Asuru AP, An M and Busenlehner LS. (2012). Dissection of Porphyrin-Induced Conformational Dynamics in the Heme Biosynthesis Enzyme Ferrochelatase. *Biochemistry* **51**, 7116-7127, doi:10.1021/bi300704c.

[34] Hansson MD, Karlberg T, Rahardja MA, Al-Karadaghi S and Hansson M. (2007). Amino Acid Residues His183 and Glu264 in Bacillus subtilis Ferrochelatase Direct and Facilitate the Insertion of Metal Ion into Protoporphyrin IX. *Biochemistry* **46**, 87-94, doi:10.1021/bi061760a.

[35] Fujishiro T and Ogawa S. (2021). The nickel-sirohydrochlorin formation mechanism of the ancestral class II chelatase CfbA in coenzyme F430 biosynthesis. *Chem Sci* **12**, 2172-2180, doi:10.1039/D0SC05439A.

[36] Romão CV, Ladakis D, Lobo SAL, Carrondo MA, Brindley AA, Deery E, Matias PM, Pickersgill RW, Saraiva LM and Warren MJ. (2011). Evolution in a family of chelatases facilitated by the introduction of active site asymmetry and protein oligomerization. *Proc Natl Acad Sci U S A* **108**, 97-102,

doi:10.1073/pnas.1014298108.

[37] Yin J, Xu LX, Cherney MM, Raux-Deery E, Bindley AA, Savchenko A, Walker JR, Cuff ME, Warren MJ and James MNG. (2006). Crystal Structure of the Vitamin B_{12} Biosynthetic Cobaltochelatase, $CbiX^S$, from *Archaeoglobus Fulgidus*. *J Struct Funct Genomics* **7**, 37-50, doi:10.1007/s10969-006-9008-x.

[38] Gabler T, Dali A, Bellei M, Sebastiani F, Becucci M, Battistuzzi G, Furtmüller PG, Smulevich G and Hofbauer S. (2024). Revisiting catalytic His and Glu residues in coproporphyrin ferrochelatase – unexpected activities of active site variants. *FEBS J* **291**, 2260-2272, doi:10.1111/febs.17101.

[39] Medlock A, Swartz L, Dailey TA, Dailey HA and Lanzilotta WN. (2007). Substrate interactions with human ferrochelatase. *Proc Natl Acad Sci U S A* **104**, 1789-1793, doi:10.1073/pnas.0606144104.

[40] Davidson RE, Chesters CJ and Reid JD. (2009). Metal ion selectivity and substrate inhibition in the metal ion chelation catalyzed by human ferrochelatase. *J Biol Chem* **284**, 33795-33799, doi:10.1074/jbc.M109.030205.

Supporting Information

Table S1. Primer sets

Figure S1. Structure and reaction of methyl pyropheophorbide *a* (Me-pyroPheide *a*) metalation.

Figure S2. Visible absorption spectra of the pigments.

Figure S3. Purified *Anaerolineae* bacterium SM23_63 (AbSGR-h) and *Arabidopsis thaliana* SGR Like (AtSGRL) proteins.

Figure S4. Mass spectrometry of the predicted metal complexes.

Figure S5. HPLC chromatogram of the pigments incubated without AbSGR-h.

Figure S6. Determination of enzymatic parameters.

Figure S7. Absorbance change of metal ions and Me-pyroPheide *a* mixture in methanol solution.

Figure S8. Pigment analysis of the reaction mixture after incubation with AbSGR-h variants.

Figure S9. Computational prediction of AbSGR-h, Zn ion, and substrate complex structure.

Figure legends

Figure 1. Insertion of metal ions into methyl pyropheophorbide *a* (Me-pyroPheide *a*) by *Anaerolineae* bacterium SM23_63 (AbSGR-h).

Purified AbSGR-h was incubated with various metal ions and Me-pyroPheide *a*, and the resulting pigments were analyzed using high-performance liquid chromatography (HPLC). Representative chromatograms are shown. A mixture without metal ions was used as a standard. Black and red arrowheads indicate Me-pyroPheide *a* and the predicted metal complexes, respectively.

Figure 2. Dechelation and chelation activities of AbSGR-h and its mutants.

(A) Dechelation activity was examined by incubating purified AbSGR-h with chlorophyll *a*, and pheophytin *a* levels were measured using HPLC. (B) Chelation activity was examined by incubating purified AbSGR-h with Zn ions and Me-pyroPheide *a*, and the Zn complexes were determined using HPLC. The controls show the results without AbSGR-h. Error bars represent the standard deviation (SD) (n = 3). $^{**}p < 0.01$ (*t*-test).

Figure 3. Dechelation and chelation activities of the plant *Arabidopsis thaliana* SGR Like (AtSGRL).

(A) AtSGRL and chlorophyll *a* were incubated, and pigments were analyzed using HPLC. (B) AtSGRL, Zn ion, and Me-pyroPheide *a* were incubated, and pigments were analyzed using HPLC. Representative chromatograms are shown.

Figure 4. Complementation of *E. coli* strain *hemH* with *AbSGR-h.*

E. coli strain *hemH* was transformed with an empty vector (control) or plasmids harboring *E. coli HemH* or *AbSGR-h* and cultured on an agar plate with or without 0.2% glucose for 2 days at 37 °C. The growth rate of control cells is low, even with glucose supplementation. Representative cultures are shown.

Fig. 1

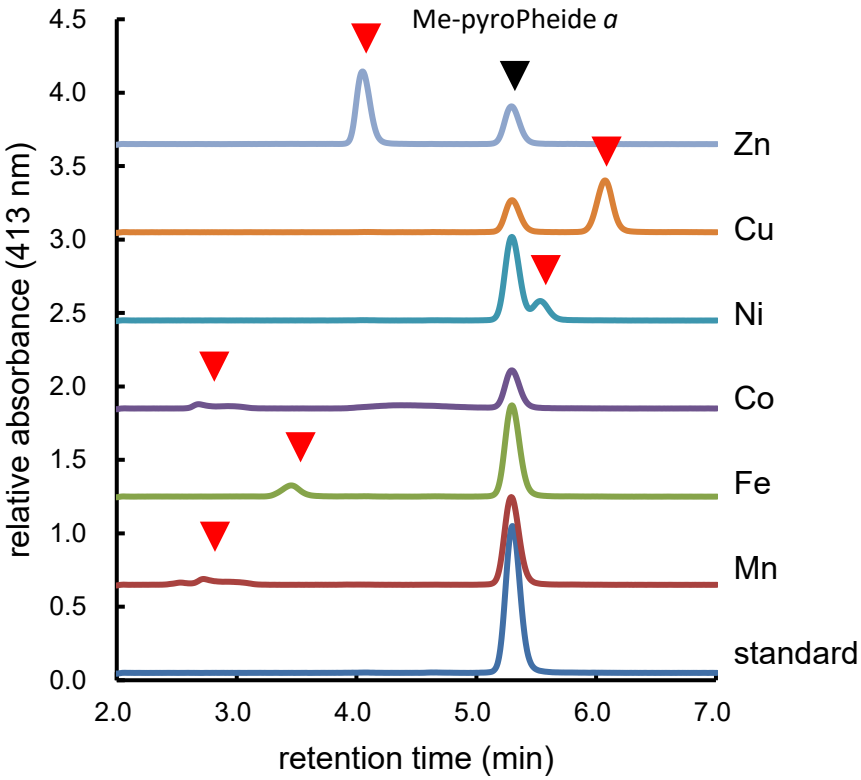
Me-pyroPheide *a*
Zn
Cu
Ni
Co
Fe
Mn
standard
relative absorbance (413 nm)
retention time (min)
4.5
4.0
3.5
3.0
2.5
2.0
1.5
1.0
0.5
0.0
2.0
3.0
4.0
5.0
6.0
7.0

Fig. 2

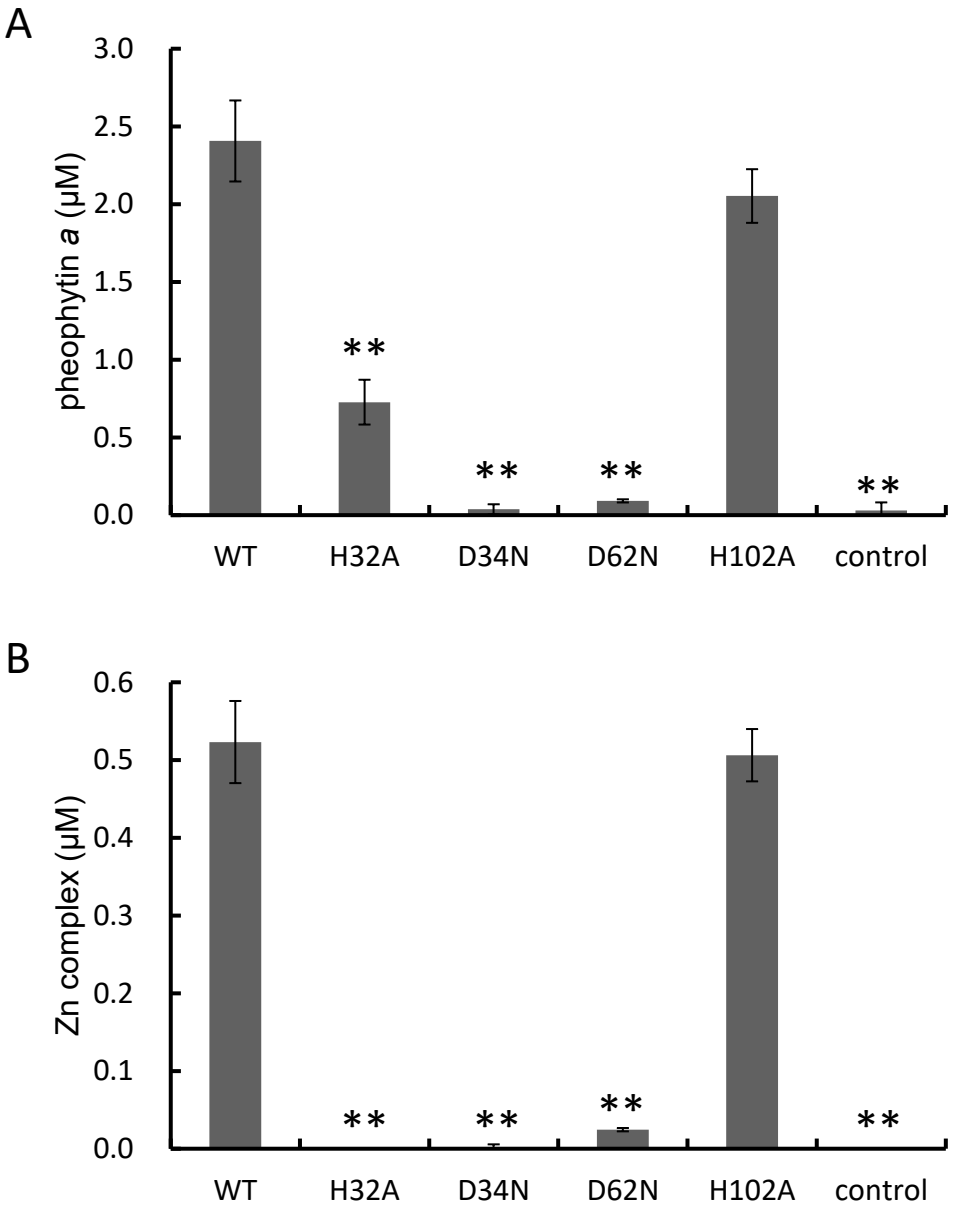
A
pheophytin a (μM)
3.0
2.5
2.0
1.5
1.0
0.5
0.0
**
**
**
**
WT
H32A
D34N
D62N
H102A
control
B
Zn complex (μM)
0.6
0.5
0.4
0.3
0.2
0.1
0.0
**
**
**
**
WT
H32A
D34N
D62N
H102A
control

Fig. 3

A

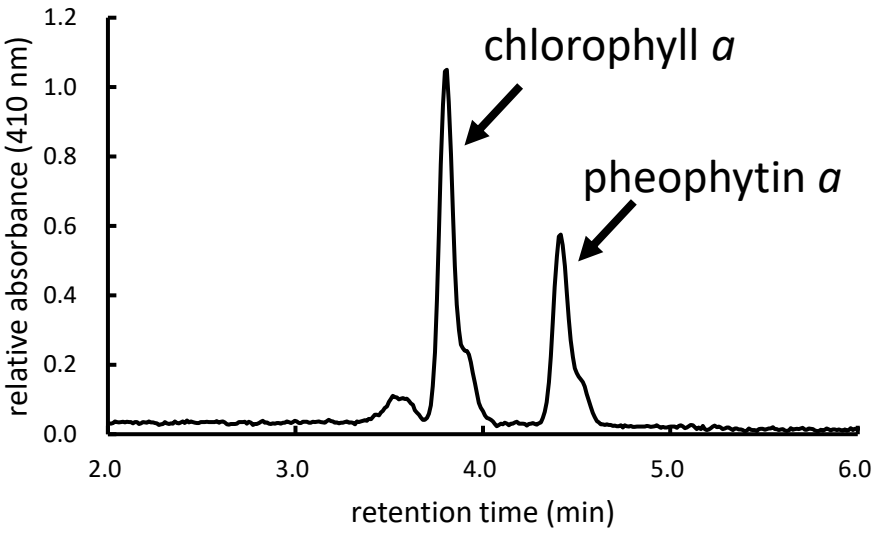
chlorophyll *a*
pheophytin *a*
relative absorbance (410 nm)
1.2
1.0
0.8
0.6
0.4
0.2
0.0
2.0
3.0
4.0
5.0
6.0
retention time (min)

B

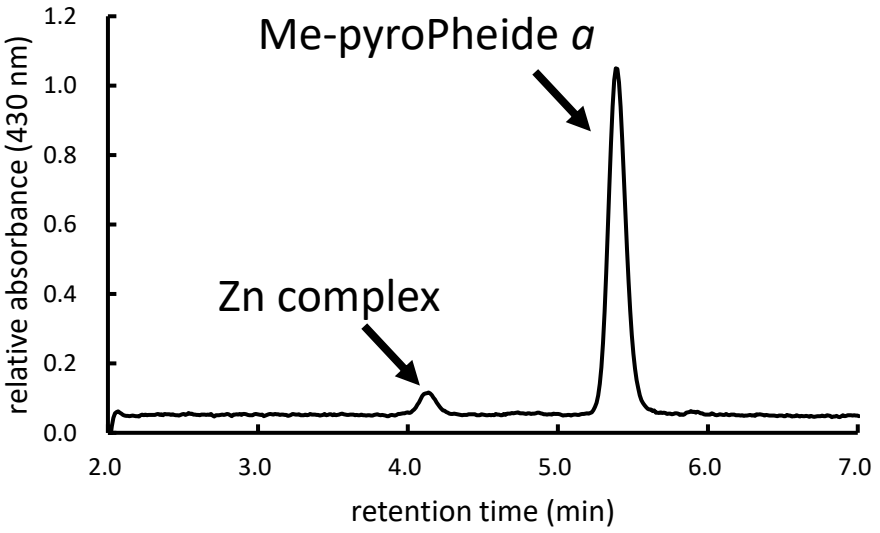
Me-pyroPheide *a*
Zn complex
relative absorbance (430 nm)
1.2
1.0
0.8
0.6
0.4
0.2
0.0
2.0
3.0
4.0
5.0
6.0
7.0
retention time (min)

Fig. 4

Table 1. Kinetics parameters of AbSGR-h with 5 μM Me-pyroPheide *a*

Metal ion	K_m (μM)	k_{cat} (min^{-1})	k_{cat}/K_m (μM^{-1} min^{-1})
Cu	2.29 ± 0.28	2.03 ± 0.12	0.89 ± 0.08
Zn	1.01 ± 0.32	2.22 ± 0.43	2.26 ± 0.35

Table 2. Kinetics parameters of AbSGR-h with 2.5 μM metal ions

Metal ion	K_m (μM)	k_{cat} (min^{-1})	k_{cat}/K_m (μM^{-1} min^{-1})
Cu	4.43 ± 0.07	2.55 ± 0.38	0.58 ± 0.01
Zn	2.46 ± 0.19	2.81 ± 0.25	1.14 ± 0.05

Table S1. Primer sets

	Sequence (5' to 3')
AbSGR-h_H102A-F	CCGCCAGGCCATGCCGCTGGTTCTGGAAGC
AbSGR-h_H102A-R	GCGGCAT**GGC**CTGGCGGAAGATTTTATCGC
AbSGR-h-pUC-F	TGATTACGCCAAGCTTAATGGATCATCTGAAACCGGA
AbSGR-h-pUC-R	GACGGCCAGTGAATTCTATTTGTAATCGCGCAGAATGC
hemH-pUC-F	ATTACGCCAAGCTTAATGCGTCAGACTAAAACCGG
hemH-pUC-R	GACGGCCAGTGAATTTTAGCGATACGCGGCAACAA

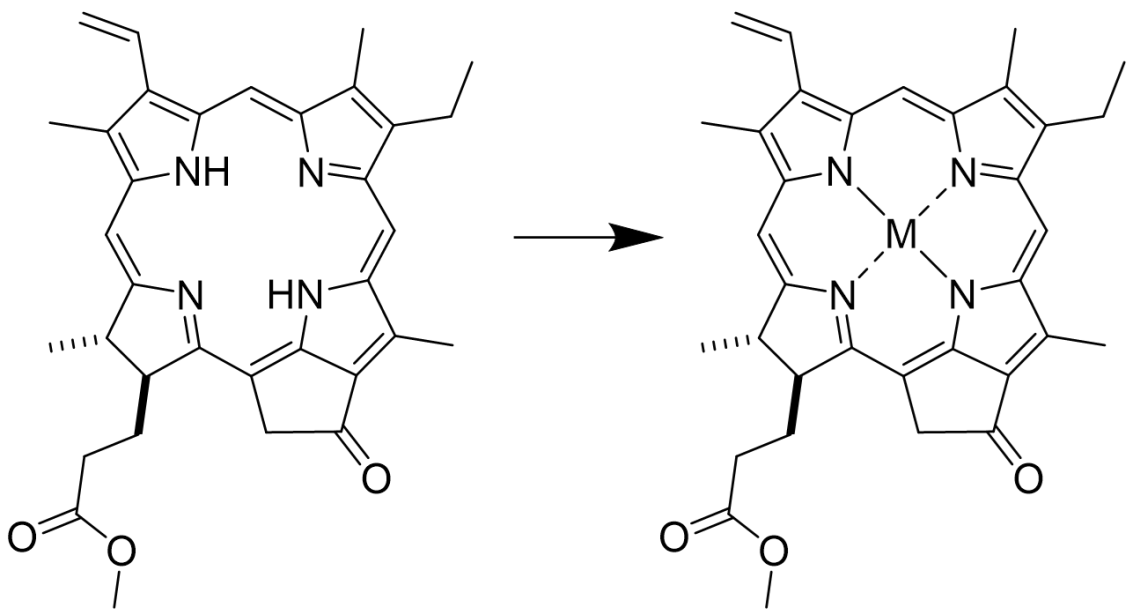

Me-pyroPheide *a* metal complex

Figure S1. Structure and reaction of methyl pyropheophorbide *a* (Me-pyroPheide *a*) metalation.
Me-pyroPheide *a* was prepared by substituting the phytyl group to a methyl group in the C17-propionate residue and removing the $C13^2$-methoxycarbonyl group from pheophytin *a*. The inserted metal ion was coordinated with the inner, four nitrogen atoms of the core chlorin.

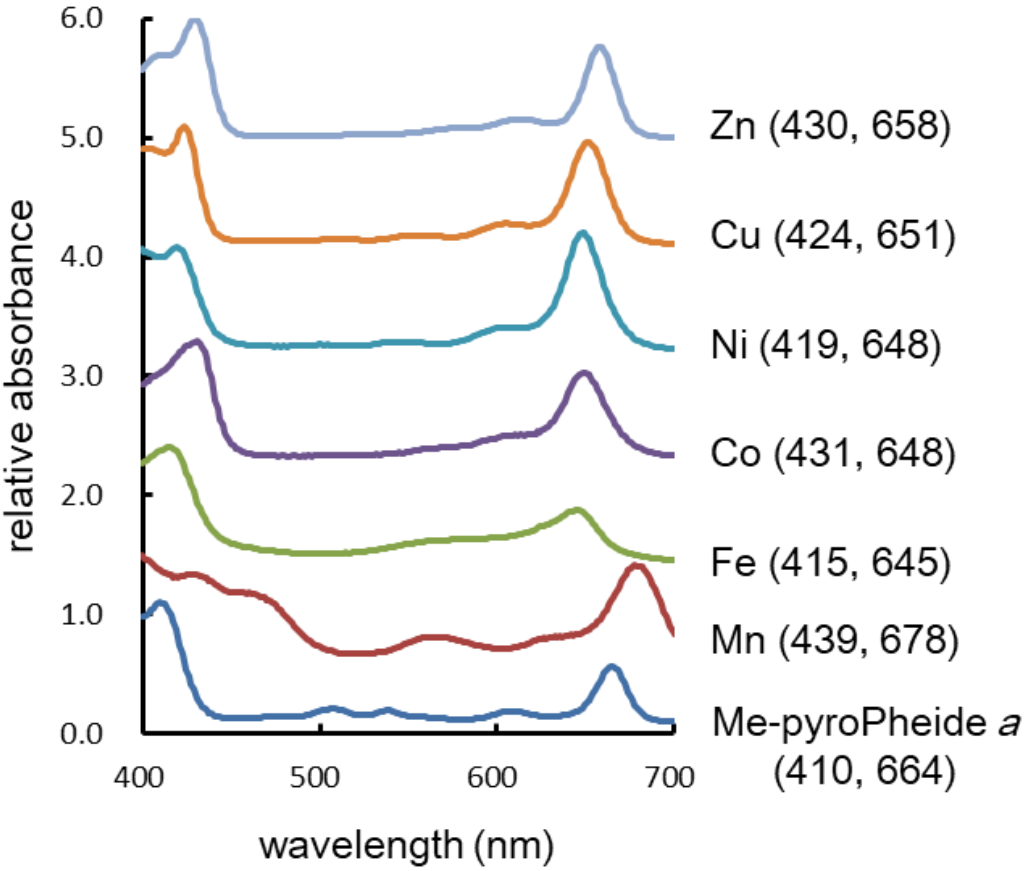

Figure S2. Visible absorption spectra of the pigments.
On-line absorption spectra of the predicted metal complex peaks of Fig. 1 obtained by normalizing the highest peak. Absorptions of the Soret and Qy bands are shown in parentheses.

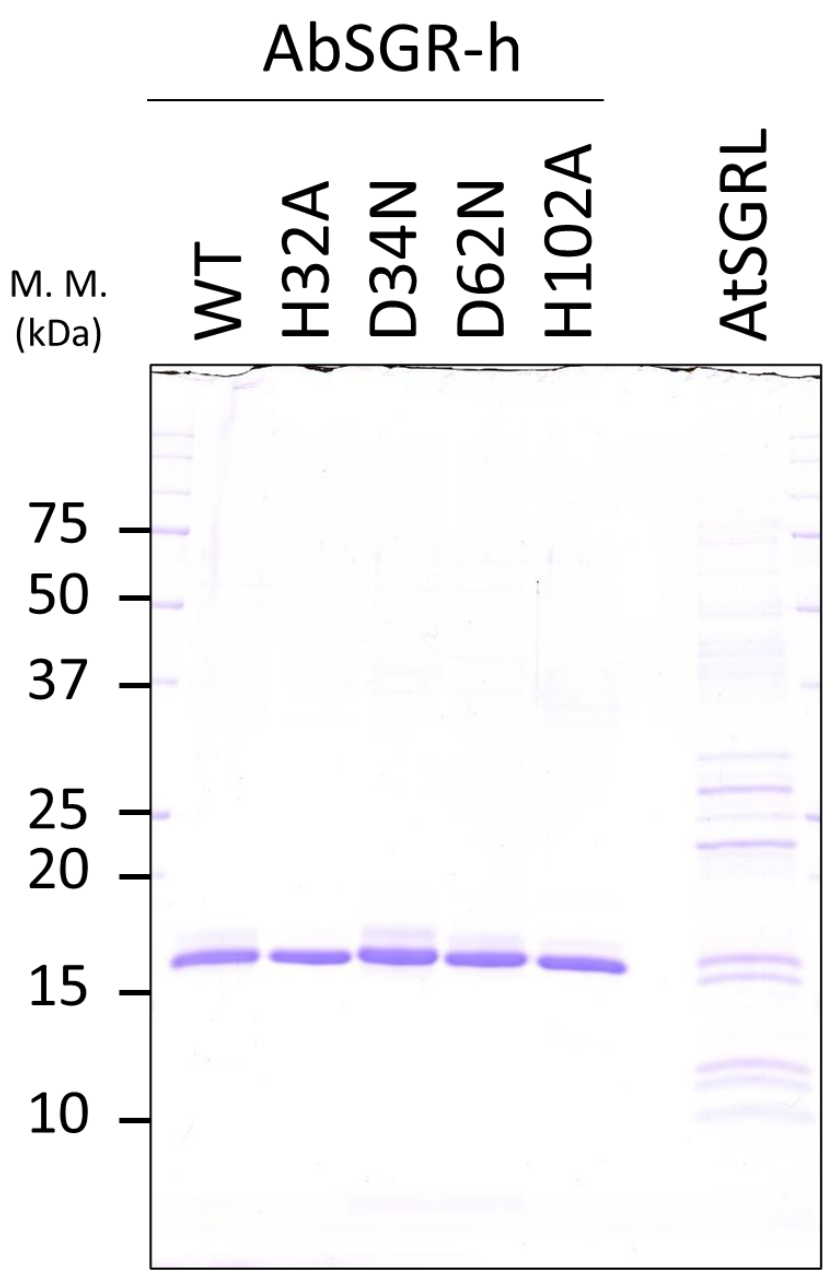

Figure S3. Purified *Anaerolineae* bacterium SM23_63 (AbSGR-h) and *Arabidopsis thaliana* SGR Like (AtSGRL) proteins.
Purified proteins were analyzed using sodium dodecyl sulfate polyacrylamide gel electrophoresis and CBB staining. AbSGR-h and its mutants (1 μg), and AtSGRL fraction protein (1.3 μg) were analyzed. A representative gel image is shown. The calculated molecular sizes of AbSGR-h and AtSGRL with the FATT tag were 18 and 39 kDa, respectively.

Me-pyroPheide *a* (*m/z* 549.3 for [*M*+H]$^+$)

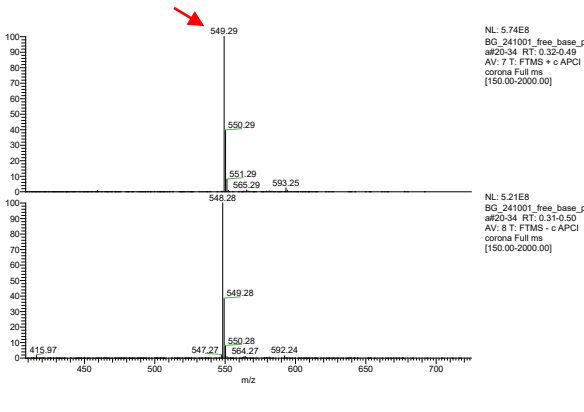

Mn complex (*m/z* 601.2 for *M*$^+$)

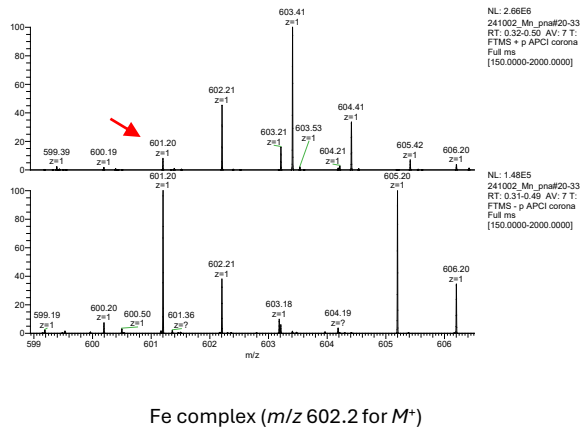

Fe complex (*m/z* 602.2 for *M*$^+$)

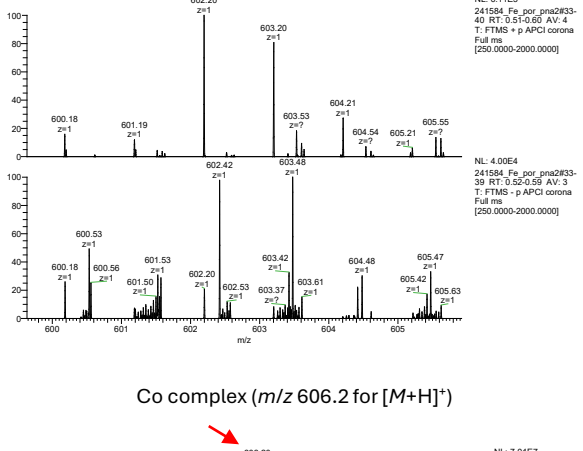

Co complex (*m/z* 606.2 for [*M*+H]$^+$)

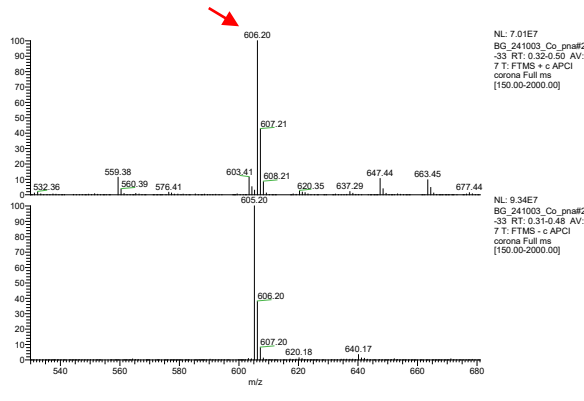

Ni complex (*m/z* 605.2 for [*M*+H]$^+$)

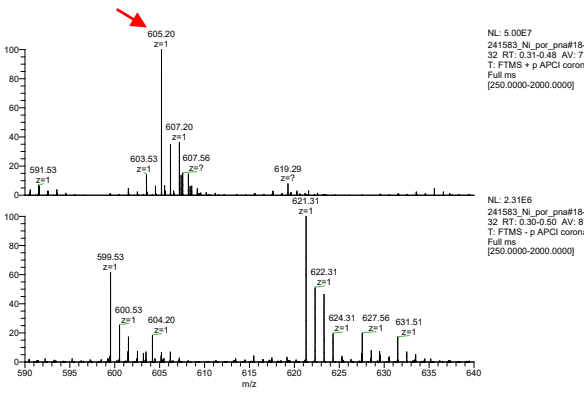

Cu complex (*m/z* 610.2 for [*M*+H]$^+$)

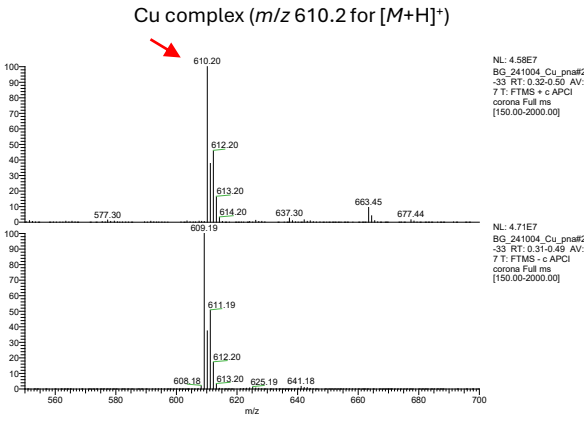

Zn complex (*m/z* 611.2 for [*M*+H]$^+$)

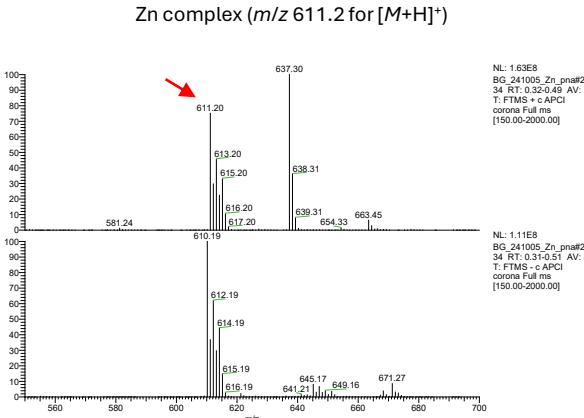

Figure S4. Mass spectrometry of the predicted metal complexes. The predicted metal complexes were isolated using high-performance liquid chromatography (HPLC) and analyzed using mass spectrometry. Positive and negative mode profiles are shown in the upper and lower panels, respectively. The observed signals with mass numbers consistent with the calculated values are marked with red arrows in the positive mode (upper panel).

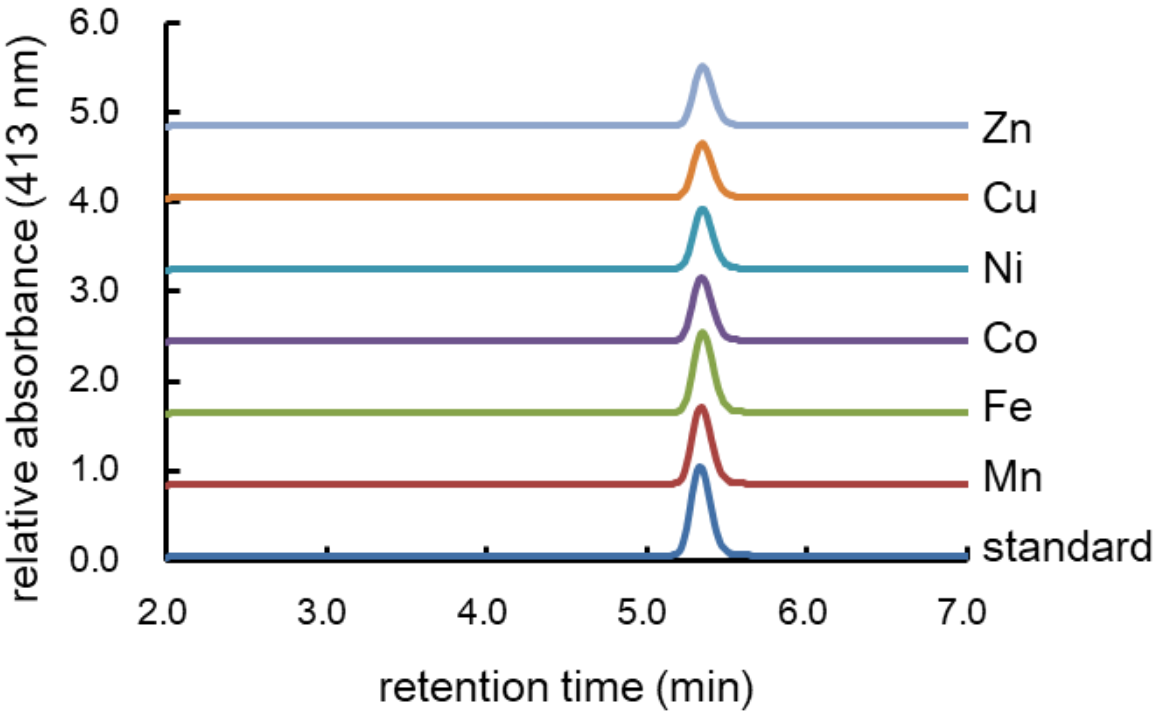

Figure S5. HPLC chromatogram of the pigments incubated without AbSGR-h. Me-pyroPheide *a* and metal ions were incubated for 15 h, and the pigments were analyzed using HPLC at 413 nm. A mixture without metal ions was used as a standard. Representative chromatograms are shown.

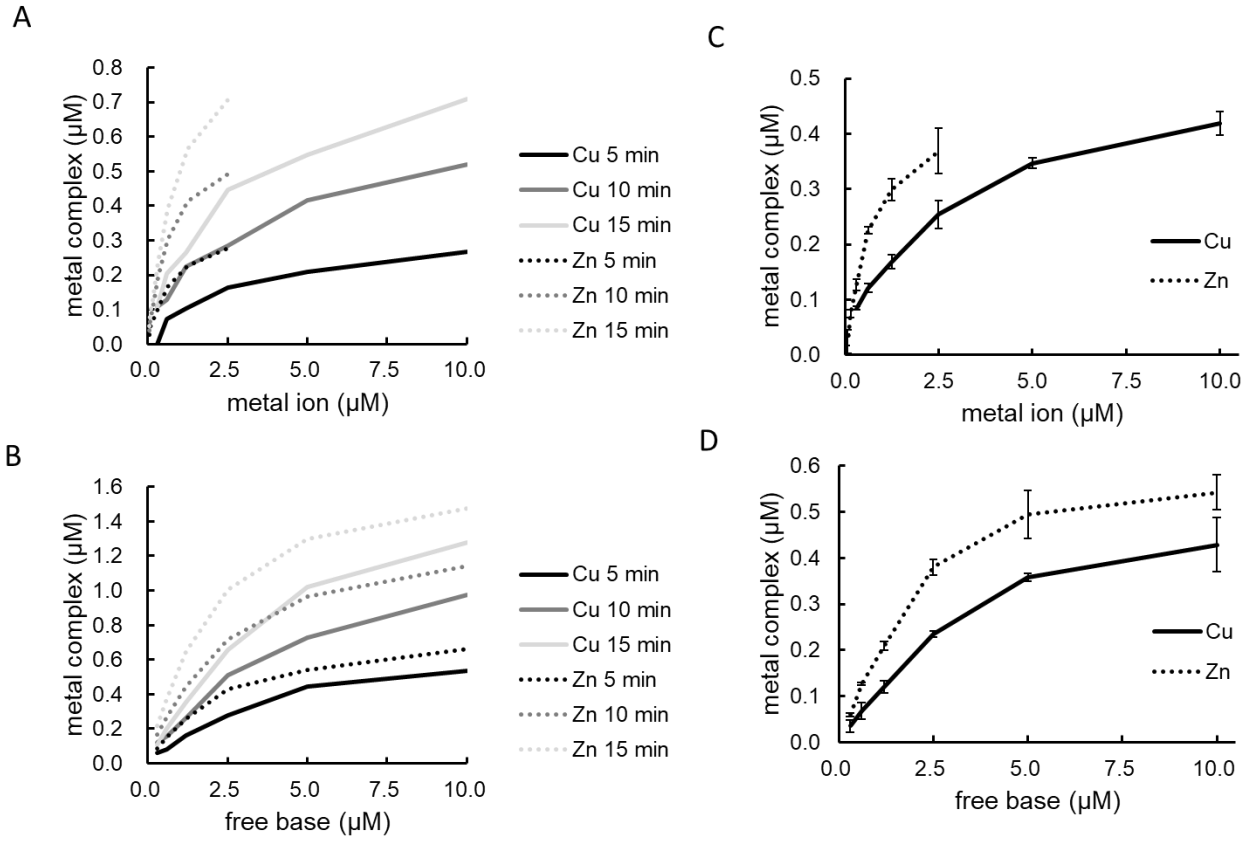

Figure S6. Determination of enzymatic parameters.
Purified AbSGR-h (0.05 μM) was incubated with different copper (Cu) or zinc (Zn) ion concentrations and 5 μM Me-pyroPheide *a* (A) or with different Me-pyroPheide *a* concentrations and 2.5 μM Cu or Zn ion (B) for 5, 10, and 15 min. Purified AbSGR-h (0.05 μM) was incubated with 5 μM Me-pyroPheide *a* and various Cu or Zn ion concentrations (C) and with 2.5 μM Cu or Zn and various Me-pyroPheide *a* concentrations (D). Error bars represent the standard deviation (n = 3). Representative results are shown. Metal complexes were determined using HPLC, and the kinetics of the enzymatic reaction were determined by fitting the data to a Michaelis–Menten plot.

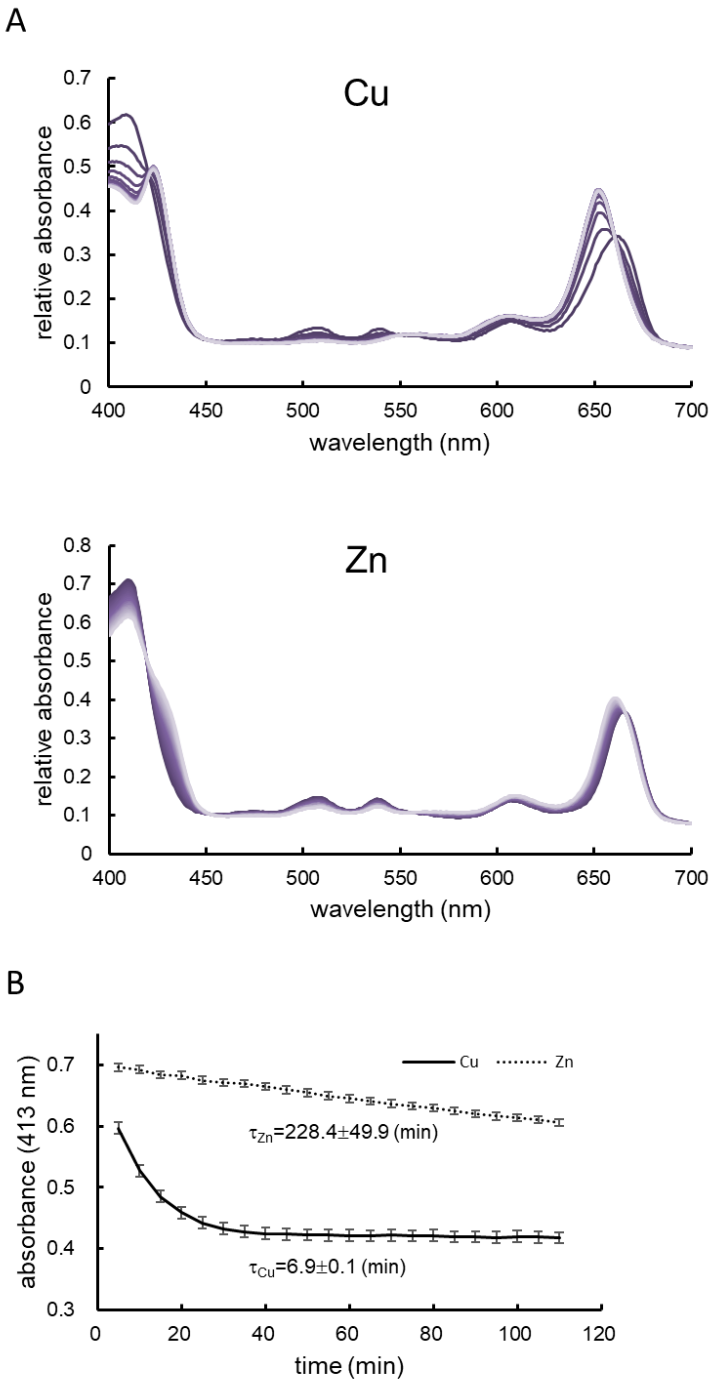

Figure S7. Absorbance change of metal ions and Me-pyroPheide *a* mixture in methanol solution.
(A) Absorption spectral change of the mixture of Me-pyroPheide *a* and Cu or Zn ions in methanol. Spectra were monitored every 5 min for 105 min. The color of the line on the graph fades with the reaction time. (B) Me-pyroPheide *a* (5 μM) and Cu or Zn ions (500 μM) were solubilized in methanol, and the change in absorbance at 413 nm was monitored every 5 min for 105 min. Error bars represent the standard deviation (n = 3). The half-time of the decay was calculated by curve fitting of the exponential decay curve. Representative results are shown.

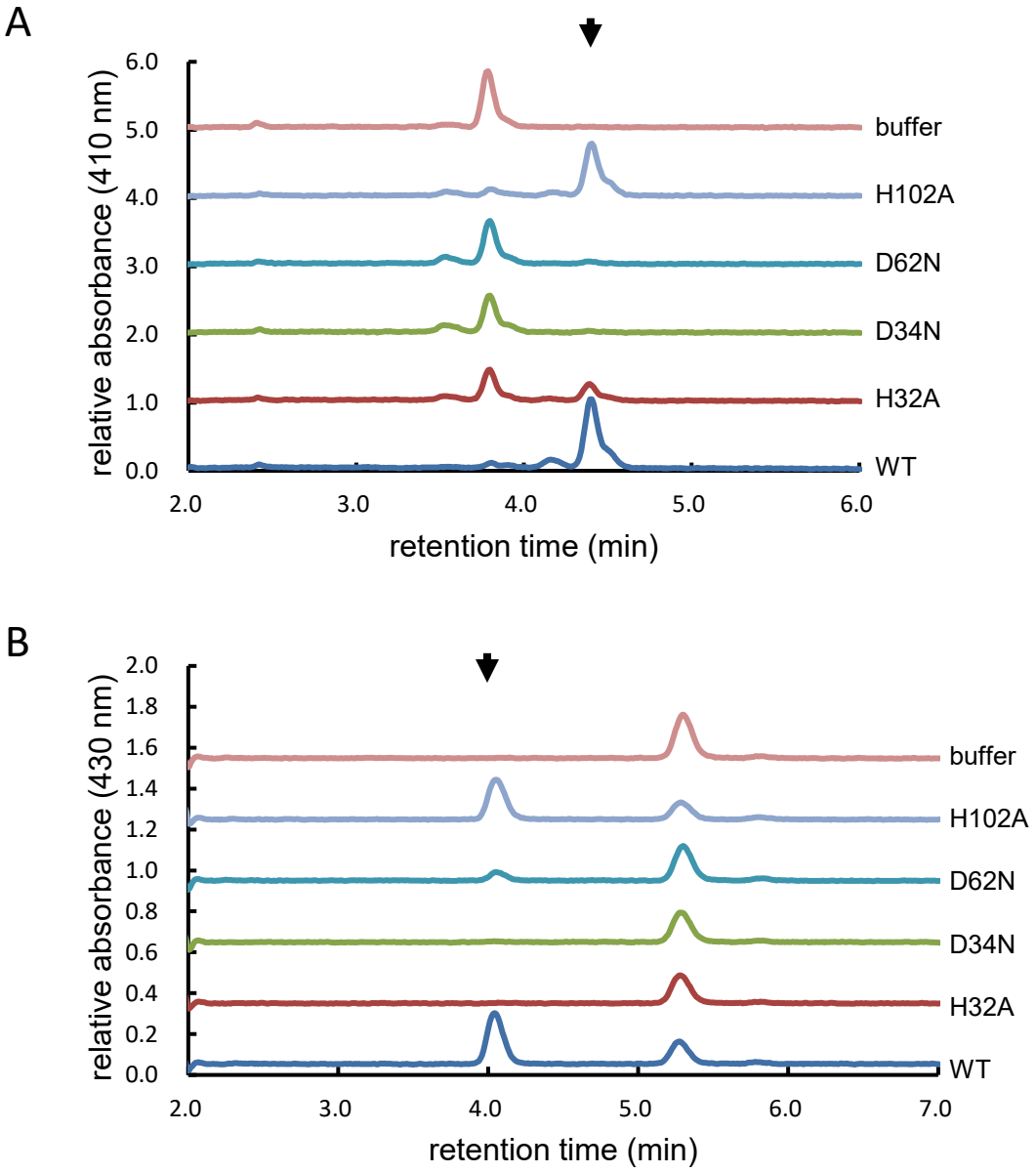

Figure S8. Pigment analysis of the reaction mixture after incubation with AbSGR-h variants.
Purified AbSGR-h and its mutant were incubated with chlorophyll *a* (A) or Zn ions and Me-pyroPheide *a* (B). After incubation, the pigments were analyzed using HPLC. Arrows indicate the products, pheophytin *a,* and the Zn complex of Me-pyroPheide *a*. Representative chromatograms are shown.

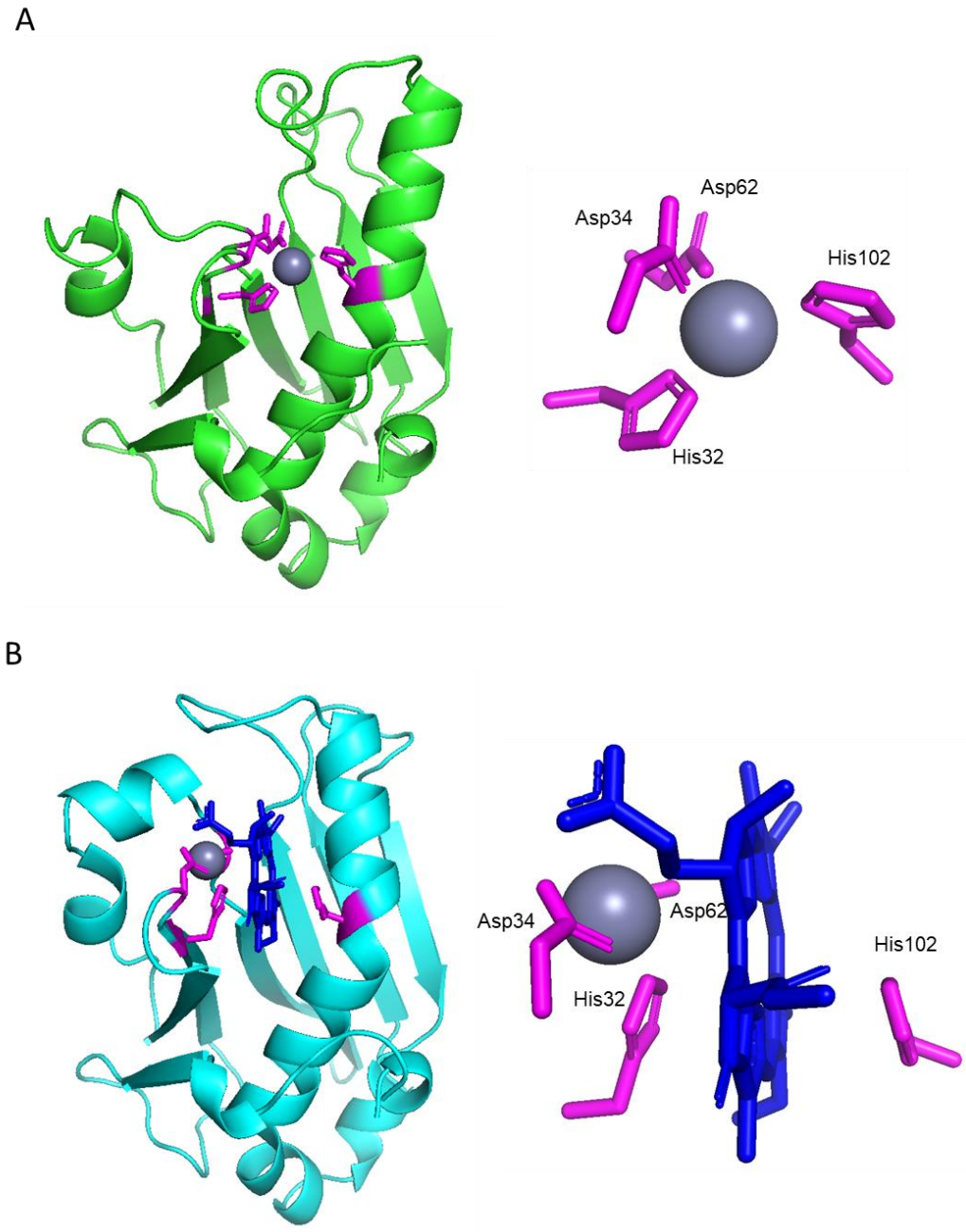

Figure S9. Computational prediction of AbSGR-h, Zn ion, and substrate complex structure.
The AbSGR-h and Zn ion (A) and AbSGR-h, Zn ion, and chlorophyll *a* complex structures (B) were predicted using AlphaFold3. Chlorophyll *a* was used instead of pheophytin derivatives because pheophytin derivatives are not available in AlphaFold3. Two Zn atoms were used as ligands for prediction. One more Zn ion was predicted to bind to the surface of the protein, which is not the catalytic site, but this was not shown. The phytyl chain was removed for ease of visualization. The Zn ions are shown as gray spheres. H32, D34, D62, and H102 are indicated in magenta. The chlorophyll *a* content is indicated in blue. The left figures show the entire structure and the right figures show the enlarged catalytic sites of the complexes.